Eur. Phys. J. C 23, 135–143 (2002)
Digital Object Identifier (DOI) 10.1007/s100520100838

THE EUROPEAN PHYSICAL JOURNAL C

The first three pomerons...

V.A. Petrov[1,a], A.V. Prokudin[1,2,3b]

[1] Institute For High Energy Physics, 142281 Protvino, Russia
[2] Dipartimento di Fisica Teorica, Università Degli Studi Di Torino, Via Pietro Giuria 1, 10125 Torino, Italy
[3] Sezione INFN di Torino, Via Pietro Giuria 1, 10125 Torino, Italy

Received: 11 July 2001 /
Published online: 20 December 2001 –

Abstract. A model of a three pomeron contribution to high energy elastic pp and $\bar{p}p$ scattering is proposed. The data are well described for all momenta ($0.01 \leq |t| \leq 14.\,\mathrm{GeV}^2$) and energies ($8. \leq s^{1/2} \leq 1800.\,\mathrm{GeV}$) ($\chi^2/\mathrm{d.o.f.} = 2.60$). The model predicts the appearance of two dips in the differential cross-section which will be measured at LHC. The parameters of the pomeron trajectories are $\alpha(0)_{\mathbb{P}_1} = 1.058$, $\alpha'(0)_{\mathbb{P}_1} = 0.560\,\mathrm{GeV}^{-2}$; $\alpha(0)_{\mathbb{P}_2} = 1.167$, $\alpha'(0)_{\mathbb{P}_2} = 0.273\,\mathrm{GeV}^{-2}$; $\alpha(0)_{\mathbb{P}_3} = 1.203$, $\alpha'(0)_{\mathbb{P}_3} = 0.094\,\mathrm{GeV}^{-2}$.

1 Introduction

Eagerly awaited high energy collisions at LHC will give access not only to yet unexplored small distances but also simultaneously to large distances that were neither explored [1]. Future measurements of total and elastic cross-sections at LHC [2] tightly related to the latter domain naturally stimulate further searches for new approaches to diffractive scattering at high energies.

Recently some models with multi-pomeron structures were proposed [3–5]. Some of these [3,4] use Born amplitudes with two pomerons as single [3] or double poles [4]. The formal violation of the Froissart–Martin bound in some of these models is considered as "practically negligible" though in terms of partial-wave amplitudes unitarity violation is flagrant at present-day energies. Nonetheless a model of such a kind [5] based on the two pomeron approach shows quite a good agreement with DIS data.

The eikonal models that are capable of describing the data for non-zero transferred momenta are developed in [6, 7]. In some cases a "generalized eikonal representation" is used [6] together with a dipole (monopole) pomeron contribution, in the others the conventional eikonal is supplemented with a "QCD motivated" part consisting of three terms [7]. It is worth noticing that the two pomeron eikonal has been applied to the description of the data more than ten years ago (see, e.g., [8]).

The very diversity of the models hints that maybe the most general way to describe high energy diffraction is just to admit an arbitrary number of pomerons (i.e. all vacuum Regge poles contributing non-negligibly at reasonably high energies. Roughly, they should have intercepts not lower than 1). On the one hand this seems to be not very economical. But on the other hand we could argue that no basic principle forbids more than one single pomeron. We could also add that in the perturbative framework the account of the renormalization group leads presumably to converting of the fixed branch point (in the J-plane) into an infinite series of simple poles accumulating down to 1 from some maximal value [9]. Unfortunately perturbative searches in this field are far from satisfactory from many viewpoints.

In this paper we would like to make a first step in the realization of the above formulated hypothesis about a many pomeron structure of the eikonal. As it seems impossible to describe the data in the framework of the eikonal approach in presence of one single pole pomeron contribution [10], and the two pomeron option does not improve the quality of the description drastically (more details are given in the text), it is fairly natural to try the next, three pomeron, option for the eikonal. We will see below that this choice appears to be rather lucky.

2 The model

Let us briefly outline the basic properties of our model. The unitarity condition is

$$\mathrm{Im}T(s,\mathbf{b}) \simeq |T(s,\mathbf{b})|^2 + \eta(s,\mathbf{b}),$$

where $T(s,\mathbf{b})$ is the scattering amplitude in the impact representation, $\mathbf{b}$ is the impact parameter, and $\eta(s,\mathbf{b})$ is the contribution of inelastic channels; this implies the following eikonal form for the scattering amplitude $T(s,\mathbf{b})$:

$$T(s,\mathbf{b}) = \frac{\mathrm{e}^{2\mathrm{i}\delta(s,\mathbf{b})} - 1}{2\mathrm{i}}, \qquad (1)$$

where $\delta(s,\mathbf{b})$ is the eikonal function. The unitarity condition in terms of the eikonal looks as follows:

[a] e-mail: petrov@mx.ihep.su
[b] e-mail: prokudin@to.infn.it

$$\mathrm{Im}\delta(s,\mathbf{b}) \geq 0, \quad s > s_{\mathrm{inel}}. \tag{2}$$

The eikonal function is assumed to have simple poles in the complex J-plane and the corresponding Regge trajectories are normally being used in the linear approximation

$$\alpha(t) = \alpha(0) + \alpha'(0)t. \tag{3}$$

Accordingly we get the following contribution (modulo the signature factor) to the eikonal function in t-space (here t is the momentum transfer):

$$\hat{\delta}(s,t) = c\left(\frac{s}{s_0}\right)^{\alpha(0)} \mathrm{e}^{t(\rho^2/4)}, \tag{4}$$

where

$$\rho^2 = 4\alpha'(0)\ln\frac{s}{s_0} + r^2 \tag{5}$$

is referred to as the "reggeon radius".

In order to relate the t- and b-spaces one proceeds via Fourier–Bessel transforms

$$\begin{aligned}\hat{f}(t) &= 4\pi s\int_0^\infty \mathrm{d}b^2 J_0(b\sqrt{-t})f(b),\\ f(b) &= \frac{1}{16\pi s}\int_{-\infty}^0 \mathrm{d}t J_0(b\sqrt{-t})\hat{f}(t).\end{aligned} \tag{6}$$

Making use of (6) we obtain the following b-representation of the eikonal function (4):

$$\delta(s,b) = \frac{c}{s_0}\left(\frac{s}{s_0}\right)^{\alpha(0)-1}\frac{\mathrm{e}^{-b^2/\rho^2}}{4\pi\rho^2}. \tag{7}$$

For the cross-sections we use the following normalizations:

$$\begin{aligned}\sigma_{\mathrm{tot}} &= \frac{1}{s}\mathrm{Im}T(s,t=0),\\ \sigma_{\mathrm{elastic}} &= 4\pi\int_0^\infty \mathrm{d}b^2|T(s,b)|^2,\\ \frac{\mathrm{d}\sigma}{\mathrm{d}t} &= \frac{|T(s,t)|^2}{16\pi s^2},\\ \rho &= \frac{\mathrm{Re}T(s,t=0)}{\mathrm{Im}T(s,t=0)}.\end{aligned} \tag{8}$$

In the present model we assume the following representation for the eikonal function:

$$\begin{aligned}\delta^{\bar{p}p}_{pp}(s,b) &= \delta^+_{\mathbb{P}_1}(s,b) + \delta^+_{\mathbb{P}_2}(s,b) + \delta^+_{\mathbb{P}_3}(s,b)\\ &\mp \delta^-_{\mathbb{O}}(s,b) + \delta^+_f(s,b) \mp \delta^-_\omega(s,b),\end{aligned} \tag{9}$$

where $\delta^+_{\mathbb{P}_{1,2,3}}(s,b)$ are pomeron contributions. "+" denotes C even trajectories (the pomeron trajectories have the following quantum numbers: 0^+J^{++}), '−' denotes C odd trajectories, $\delta^-_{\mathbb{O}}(s,b)$ is the odderon contribution (the odderon is the C odd partner of the pomeron with quantum numbers 0^-J^{--}); δ^+_f, $\delta^-_\omega(s,b)$ are the contributions of secondary reggeons, f ($C=+1$) and ω ($C=-1$).

The form (4) is not compatible with crossing symmetry, which is easily restored by the substitution $s \to s\mathrm{e}^{-\mathrm{i}\pi/2}$. We introduce a new dimensionless variable

$$\tilde{s} = \frac{s}{s_0}\mathrm{e}^{-\mathrm{i}\pi/2}, \tag{10}$$

and obtain each $C+$ and $C-$ contribution with its appropriate signature factor and the form:

$$\begin{aligned}\delta^+(s,b) &= \mathrm{i}\frac{c}{s_0}\tilde{s}^{\alpha(0)-1}\frac{\mathrm{e}^{-b^2/\rho^2}}{4\pi\rho^2},\\ \rho^2 &= 4\alpha'(0)\ln\tilde{s} + r^2 \quad (C=+1);\end{aligned} \tag{11}$$

$$\begin{aligned}\delta^-(s,b) &= \frac{c}{s_0}\tilde{s}^{\alpha(0)-1}\frac{\mathrm{e}^{-b^2/\rho^2}}{4\pi\rho^2},\\ \rho^2 &= 4\alpha'(0)\ln\tilde{s} + r^2 \quad (C=-1).\end{aligned} \tag{12}$$

The parameters of secondary reggeon trajectories are fixed according to the parameters obtained from a fit of the meson spectrum [11]:

$$\begin{aligned}\alpha_f(t) &= 0.69 + 0.84t,\\ \alpha_\omega(t) &= 0.47 + 0.93t.\end{aligned} \tag{13}$$

All the trajectories are taken in the linear approximation

$$\alpha_i(t) = \alpha_i(0) + \alpha_i'(0)t \quad (i = \mathbb{P}_1, \mathbb{P}_2, \mathbb{P}_3, \mathbb{O}). \tag{14}$$

Let us remark that all good fits require $\alpha_{\mathbb{P}}(0) - 1 \equiv \Delta_{\mathbb{P}} > 0$, which means that the Born amplitude will eventually exceed the Froissart–Martin [12] unitarity bound. This violation of unitarity is removed by all kinds of "eikonalization". Nevertheless, one must take into account the following unitarity constraints [13]:

$$\alpha_{\mathbb{P}}(0) \geq \alpha_{\mathbb{O}}(0) \quad \text{and} \quad \alpha'_{\mathbb{P}}(0) \geq \alpha'_{\mathbb{O}}(0), \tag{15}$$

where $\mathbb{P}$ is the leading pomeron trajectory (the one with the highest intercept $\Delta_{\mathbb{P}}$).

3 Results

We fit the adjustable parameters over a set of 982 pp and $\bar{p}p$ data of both forward observables (the total cross-sections σ_{tot}, and ρ the ratios of real to imaginary part of the amplitude) in the range $8. \leq s^{1/2} \leq 1800.\,\mathrm{GeV}$ and angular distributions ($\mathrm{d}\sigma/\mathrm{d}t$) in the ranges $23. \leq s^{1/2} \leq 1800.\,\mathrm{GeV}$, $0.01 \leq |t| \leq 14.\,\mathrm{GeV}^2$.

It is instructive to start with the two pomeron option. We give corresponding results in Figs. 1, 2, 3, 4 and 5. In this case we use 16 parameters and achieve $\chi^2/\mathrm{d.o.f.} = 10.87$. The parameters obtained in the two pomeron option are presented in Table 1 (all the errors are obtained according to MINUIT output). The description of the data is still unsatisfactory, though it is better than in the case of one pomeron contribution to the eikonal function [10].

Now let us consider the results of the three pomeron option. Having used 20 adjustable parameters we achieved

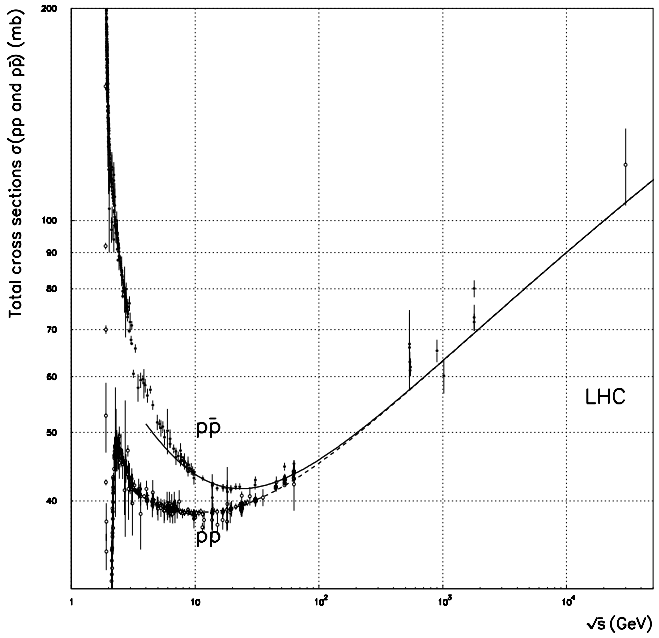

Fig. 1. Total cross-sections of pp scattering (hollow circles) and $\bar{p}p$ scattering (full circles) and curves corresponding to their description in the two pomeron model

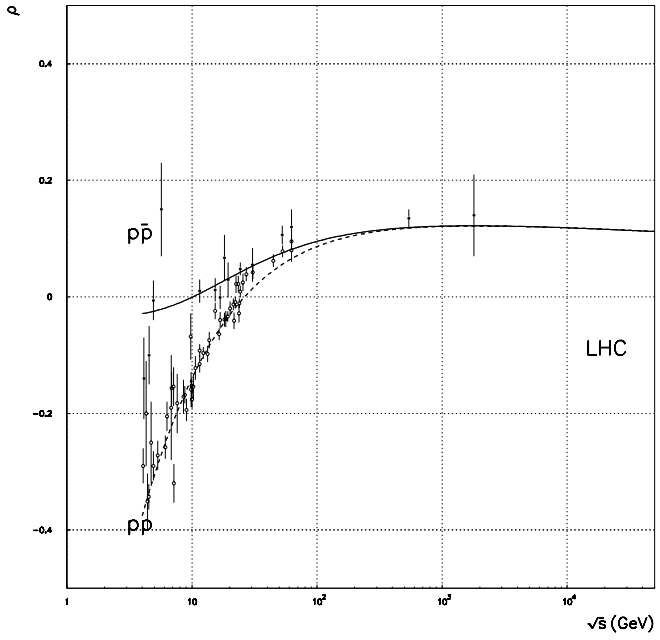

Fig. 2. Ratios of the real to the imaginary part of the forward pp scattering amplitude (hollow circles) and $\bar{p}p$ scattering amplitude (full circles) and curves corresponding to their description in the two pomeron model

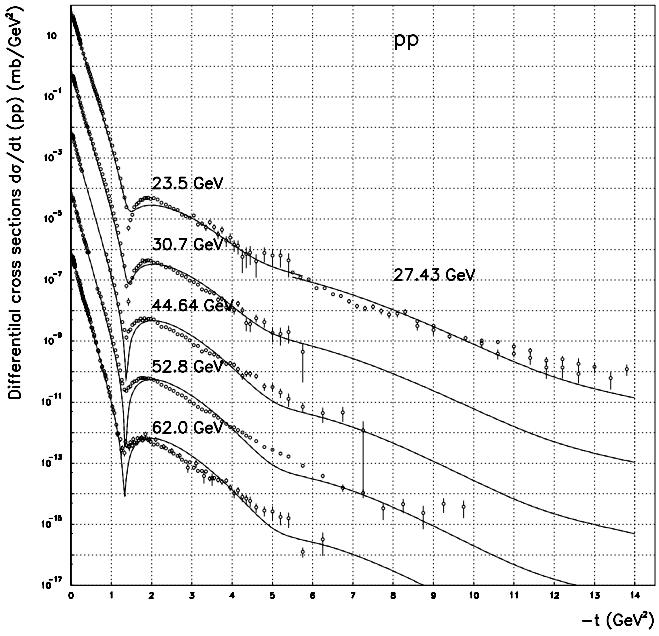

Fig. 3. Differential cross-sections for pp scattering and curves corresponding to their description in the two pomeron model. A factor 10^{-2} between each successive set of data is omitted

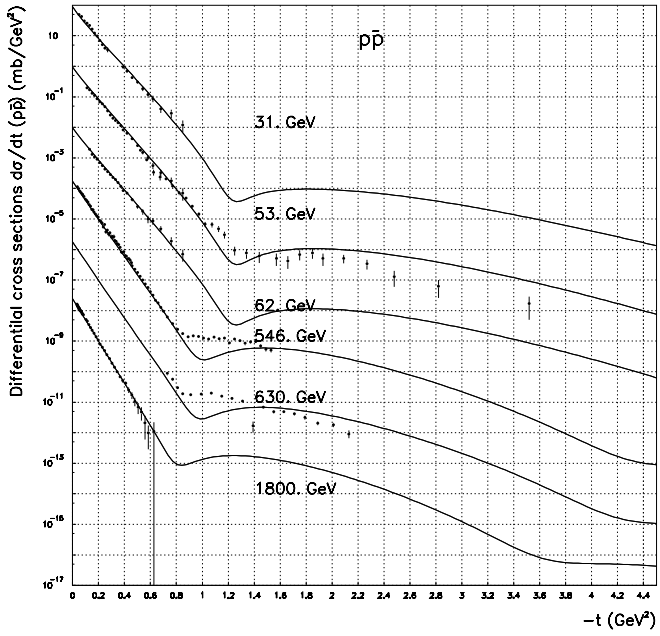

Fig. 4. Differential cross-sections for $\bar{p}p$ scattering and curves corresponding to their description in the two pomeron model. A factor 10^{-2} between each successive set of data is omitted

χ^2/d.o.f. = 2.60. The parameters are presented in Table 2 (all the errors are obtained according to MINUIT output).

The results are shown in Figs. 6, 7, 8, 9, 10, 11, 12 and 13.

We do not include elastic cross-section data sets into the fit and predictions of the model for elastic cross-sections can be seen in Fig. 7.

In order to estimate the quality of the description, we have calculated partial χ^2 over all sets of data used in the fit. This χ^2 is calculated using the following formula:

$$\chi^2 = \sum_{n=1}^{\text{ntot}} \frac{(\sigma_{\text{theory}}(n) - \sigma_{\text{exp}}(n))^2}{(\Delta(\sigma_{\text{exp}}(n)))^2}, \qquad (16)$$

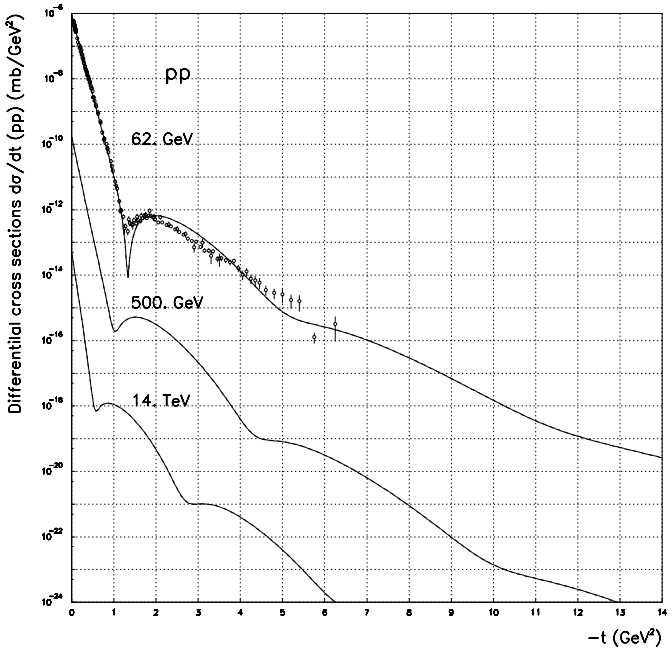

Fig. 5. Predictions of the two pomeron model for the differential cross-section of pp scattering which will be mesured at LHC with $s^{1/2} = 14.\,\mathrm{TeV}$ and at RHIC $s^{1/2} = 500.\,\mathrm{GeV}$. The data corresponding to the energy $s^{1/2} = 62.\,\mathrm{GeV}$ is multiplied by 10^{-8}, RHIC by 10^{-12}, and that of LHC by 10^{-16}

Table 1. Parameters obtained by fitting to the data with two pomeron contributions

	Pomeron$_1$		f-reggeon
$\Delta_{\mathbb{P}_1}$	0.0859 ± 0.0021	Δ_f	-0.31 (FIXED)
$c_{\mathbb{P}_1}$	53.18 ± 0.86	c_f	188.51 ± 12.13
$\alpha'_{\mathbb{P}_1}$	$0.360 \pm 0.009\,\mathrm{GeV}^{-2}$	α'_f	$0.84\,\mathrm{GeV}^{-2}$ (FIXED)
$r^2_{\mathbb{P}_1}$	$9.595 \pm 0.6289\,\mathrm{GeV}^{-2}$	r^2_f	$41.424 \pm 7.971\,\mathrm{GeV}^{-2}$
	Pomeron$_2$		ω-reggeon
$\Delta_{\mathbb{P}_2}$	0.14437 ± 0.0051	Δ_ω	-0.53 (FIXED)
$c_{\mathbb{P}_2}$	6.87 ± 0.36	c_ω	-171.36 ± 8.23
$\alpha'_{\mathbb{P}_2}$	$0.082 \pm 0.004\,\mathrm{GeV}^{-2}$	α'_ω	$0.93\,\mathrm{GeV}^{-2}$ (FIXED)
$r^2_{\mathbb{P}_2}$	$4.765 \pm 0.2533\,\mathrm{GeV}^{-2}$	r^2_ω	$2.621 \pm 6.362\,\mathrm{GeV}^{-2}$
	Odderon		
$\Delta_{\mathbb{O}}$	-0.2707 ± 0.1178	s_0	$1.0\,\mathrm{GeV}^2$ (FIXED)
$c_{\mathbb{O}}$	1.8134 ± 1.4837		
$\alpha'_{\mathbb{O}}$	$0.029 \pm 0.023\,\mathrm{GeV}^{-2}$		
$r^2_{\mathbb{O}}$	$1.159 \pm 0.591\,\mathrm{GeV}^{-2}$		

where ntot is the number of data in the set, σ_{exp} is the experimental value of the quantity that is described, σ_{theory} is our prediction for this quantity, and $\Delta(\sigma_{\mathrm{exp}}(n))$ is the experimental uncertainty.

In the sets of data corresponding to total cross-sections and to ratios of real to imaginary parts of the forward scattering amplitude we discarded those experimental points which gave a contribution of more than 2. to the χ^2. Having performed such an analysis we found that there were 10 such points out of 43 in the $\bar{p}p$ total cross-section set and the resulting χ^2 was reduced by a factor of 2.6 from 1.83 to 0.71; there were 11 such points out of 79 in the pp total cross-section set and the resulting χ^2 was reduced by a factor of 2.9 from 1.06 to 0.36; there were 14 such points out of 62 in the pp ρ set and the resulting χ^2 was reduced by a factor of 3.5 from 1.52 to 0.43, and in the $\bar{p}p$ ρ set there were no such points.

Table 2. Parameters obtained by fitting to the data

	Pomeron$_1$		f-reggeon
$\Delta_{\mathbb{P}_1}$	0.0578 ± 0.0020	Δ_f	-0.31 (FIXED)
$c_{\mathbb{P}_1}$	53.007 ± 0.795	c_f	191.69 ± 2.12
$\alpha'_{\mathbb{P}_1}$	$0.5596 \pm 0.0078\,\mathrm{GeV}^{-2}$	α'_f	$0.84\,\mathrm{GeV}^{-2}$ (FIXED)
$r^2_{\mathbb{P}_1}$	$6.3096 \pm 0.2522\,\mathrm{GeV}^{-2}$	r^2_f	$31.593 \pm 1.099\,\mathrm{GeV}^{-2}$
	Pomeron$_2$		ω-reggeon
$\Delta_{\mathbb{P}_2}$	0.1669 ± 0.0012	Δ_ω	-0.53 (FIXED)
$c_{\mathbb{P}_2}$	9.6762 ± 0.1600	c_ω	-174.18 ± 2.72
$\alpha'_{\mathbb{P}_2}$	$0.2733 \pm 0.0056\,\mathrm{GeV}^{-2}$	α'_ω	$0.93\,\mathrm{GeV}^{-2}$ (FIXED)
$r^2_{\mathbb{P}_2}$	$3.1097 \pm 0.1817\,\mathrm{GeV}^{-2}$	r^2_ω	$7.467 \pm 1.083\,\mathrm{GeV}^{-2}$
	Pomeron$_3$		
$\Delta_{\mathbb{P}_3}$	0.2032 ± 0.0041	s_0	$1.0\,\mathrm{GeV}^2$ (FIXED)
$c_{\mathbb{P}_3}$	1.6654 ± 0.0669		
$\alpha'_{\mathbb{P}_3}$	$0.0937 \pm 0.0029\,\mathrm{GeV}^{-2}$		
$r^2_{\mathbb{P}_3}$	$2.4771 \pm 0.0964\,\mathrm{GeV}^{-2}$		
	Odderon		
$\Delta_{\mathbb{O}}$	0.19200 ± 0.0025		
$c_{\mathbb{O}}$	0.0166 ± 0.0022		
$\alpha'_{\mathbb{O}}$	$0.048 \pm 0.0027\,\mathrm{GeV}^{-2}$		
$r^2_{\mathbb{O}}$	$0.1398 \pm 0.0570\,\mathrm{GeV}^{-2}$		

The partial χ^2 may be found in Table 3.

Some of these χ^2s are high (for instance, those for differential cross-sections at $s^{1/2} = 53,\,630\,\mathrm{GeV}$). This reflects the fact that we did not make use of systematical errors for these sets of data which can be as high as 30%.

4 Conclusion and discussion

Above we have developed a model which is based on the general argument of multiplicity of the pomeron Regge poles in the eikonal. The present model shows a very good description of the available data for all momenta ($0.01 \leq |t| \leq 14.\,\mathrm{GeV}^2$) and energies ($8. \leq s^{1/2} \leq 1800.\,\mathrm{GeV}$); we find that $\chi^2/\mathrm{d.o.f.} = 2.60$.

The model predicts the appearance of two dips in the differential cross-section which will be measured at LHC, see Fig. 13, and this prediction is stable in the sense that all two models with two and three pomeron contributions predict the same behavior of the differential cross-section with two dips. These dips are to appear in the region $t_1 \simeq$

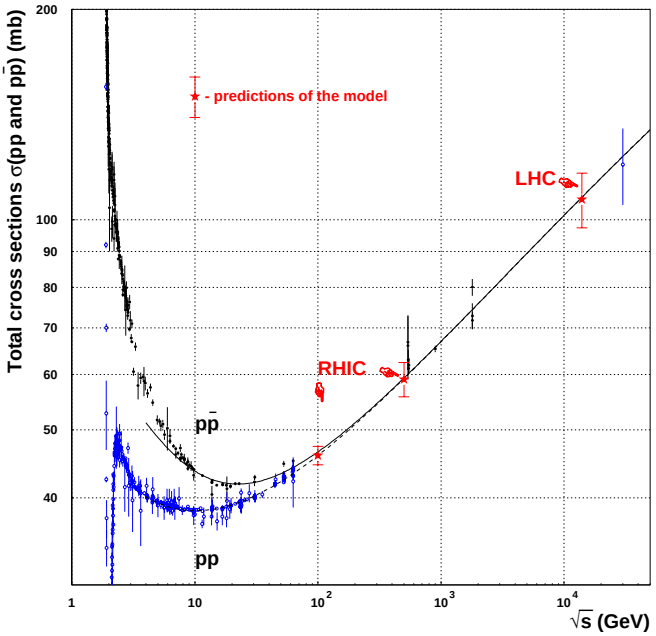

Fig. 6. Total cross-sections of pp scattering (hollow circles) and $\bar{p}p$ scattering (full circles) and curves corresponding to their description in the three pomeron model

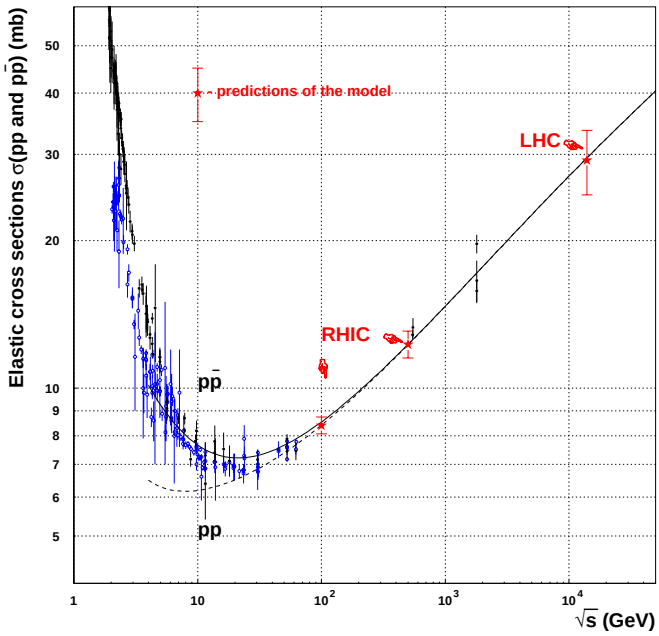

Fig. 7. Elastic cross-sections of pp scattering (hollow circles) and $\bar{p}p$ scattering (full circles) and curves corresponding to their description in the three pomeron model. These sets of data are not included in the fit

Table 3. Partial χ^2

	Set of data	Number of points, ntot	χ^2/ntot
1	$\sigma^{\bar{p}p}_{\text{total}}$	33	0.7167
2	$\sigma^{pp}_{\text{total}}$	68	0.3617
3	$\rho^{\bar{p}p}$	11	0.6086
4	ρ^{pp}	48	0.4326
5	$d\sigma/dt^{\bar{p}p}$, $\sqrt{s} = 31.\,\text{GeV}$	22	3.3688
6	$d\sigma/dt^{\bar{p}p}$, $\sqrt{s} = 53.\,\text{GeV}$	52	8.5447
7	$d\sigma/dt^{\bar{p}p}$, $\sqrt{s} = 62.\,\text{GeV}$	23	1.8524
8	$d\sigma/dt^{\bar{p}p}$, $\sqrt{s} = 546.\,\text{GeV}$	78	3.8425
9	$d\sigma/dt^{\bar{p}p}$, $\sqrt{s} = 630.\,\text{GeV}$	19	9.9273
10	$d\sigma/dt^{\bar{p}p}$, $\sqrt{s} = 1800.\,\text{GeV}$	51	1.3741
11	$d\sigma/dt^{pp}$, $\sqrt{s} = 23.5\,\text{GeV}$	105	2.2491
12	$d\sigma/dt^{pp}$, $\sqrt{s} = 27.43\,\text{GeV}$	39	1.8929
13	$d\sigma/dt^{pp}$, $\sqrt{s} = 30.7\,\text{GeV}$	92	4.4559
14	$d\sigma/dt^{pp}$, $\sqrt{s} = 44.64\,\text{GeV}$	97	1.5748
15	$d\sigma/dt^{pp}$, $\sqrt{s} = 52.8\,\text{GeV}$	93	2.0956
16	$d\sigma/dt^{pp}$, $\sqrt{s} = 62.\,\text{GeV}$	151	2.4272
	Number of parameters	Total number of points	χ^2/d.o.f.
	20	982	2.6031

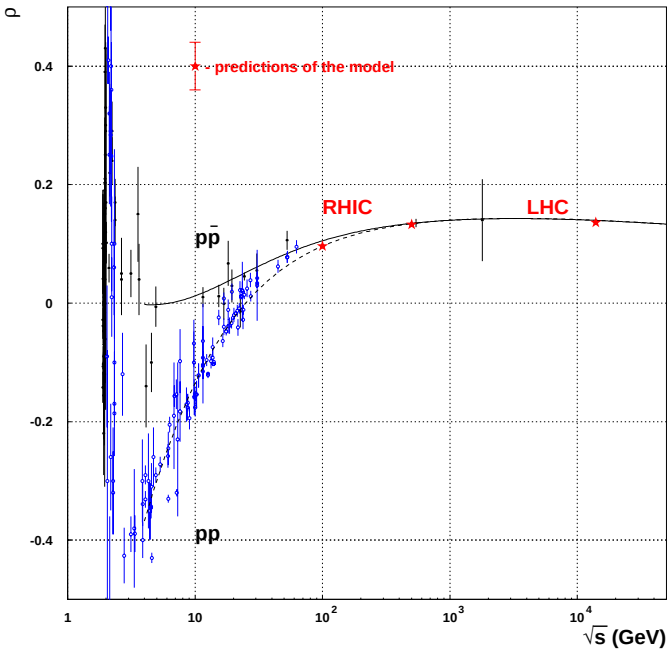

Fig. 8. Ratios of the real to the imaginary part of the forward pp scattering amplitude (hollow circles) and $\bar{p}p$ scattering amplitude (full circles) and curves corresponding to their description in the three pomeron model

$-0.5\,\text{GeV}^2$ and $t_2 \simeq -2.5\,\text{GeV}^2$ which is in agreement with other predictions [6,15].

In the high $|t|$ domain the model shows predominance of the odderon contribution and its interference with the pomeron$_3$ contribution, and this predominance of the odderon is in agreement with the model of [16] based on assumptions different from ours.

We predict the following values of the total cross-section, elastic cross-section, and the ratio of real to imaginary part of the amplitude for the LHC:

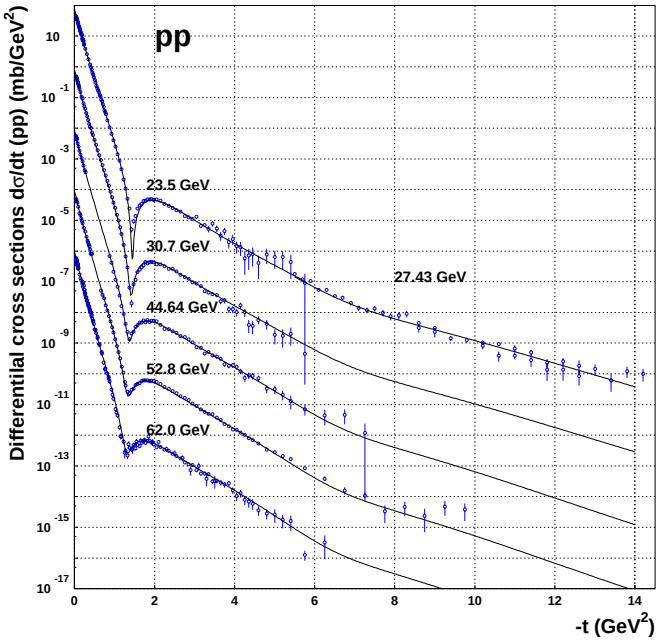

Fig. 9. Differential cross-sections for pp scattering and curves corresponding to their description in the three pomeron model. A factor 10^{-2} between each successive set of data is omitted

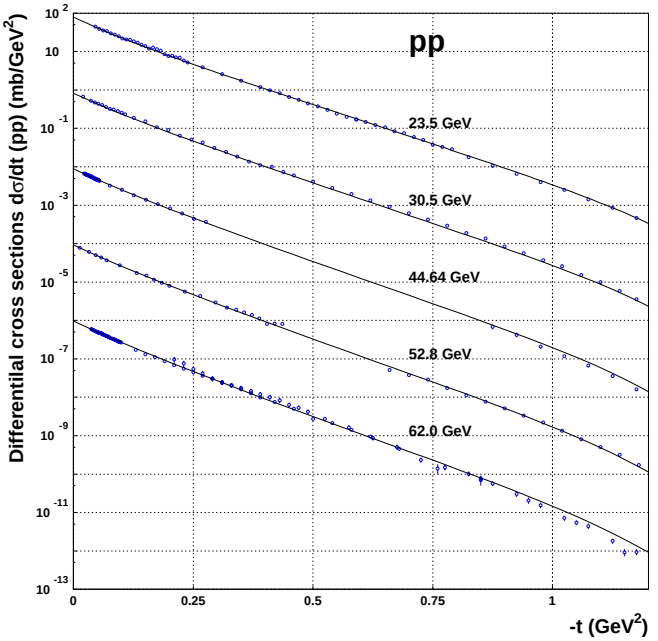

Fig. 10. Differential cross-sections for pp scattering in the region of small momenta $0.01 \leq |t| \leq 1.2\,\mathrm{GeV}^2$ and curves corresponding to their description in the three pomeron model. A factor 10^{-2} between each successive set of data is omitted

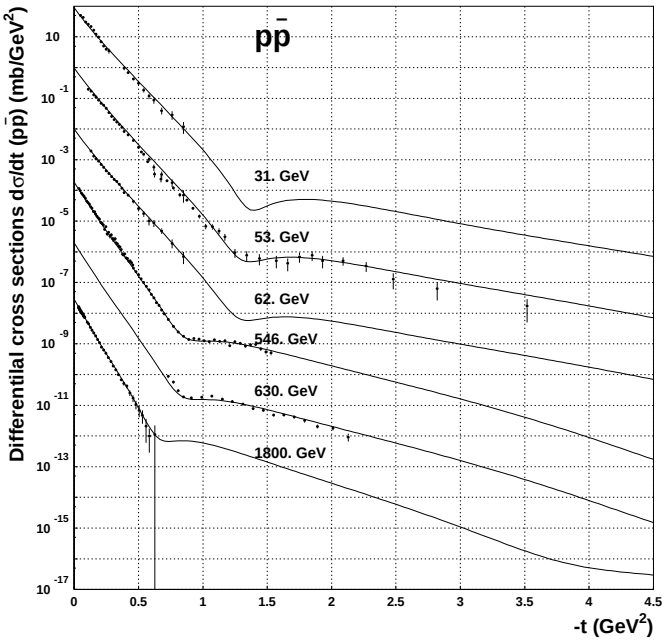

Fig. 11. Differential cross-sections for $\bar{p}p$ scattering and curves corresponding to their description in the three pomeron model. A factor 10^{-2} between each successive set of data is omitted

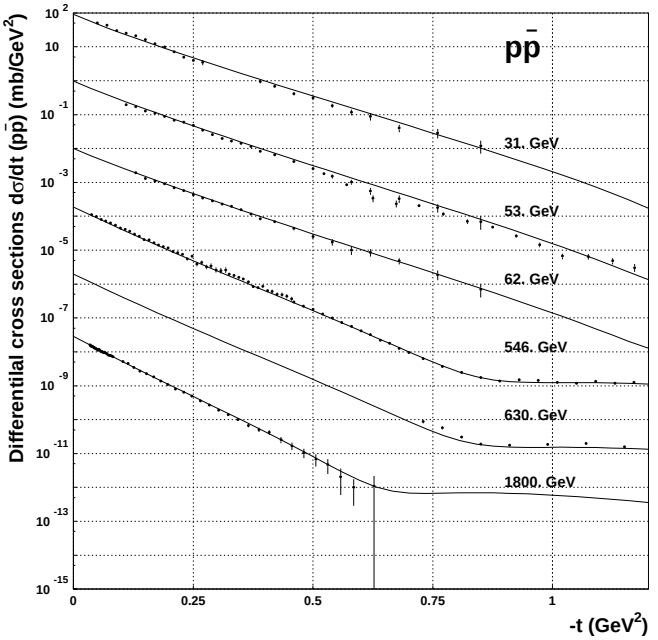

Fig. 12. Differential cross-sections for pp scattering in the region of small momenta $0.01 \leq |t| \leq 1.2\,\mathrm{GeV}^2$ and curves corresponding to their description in the three pomeron model. A factor 10^{-2} between each successive set of data is omitted

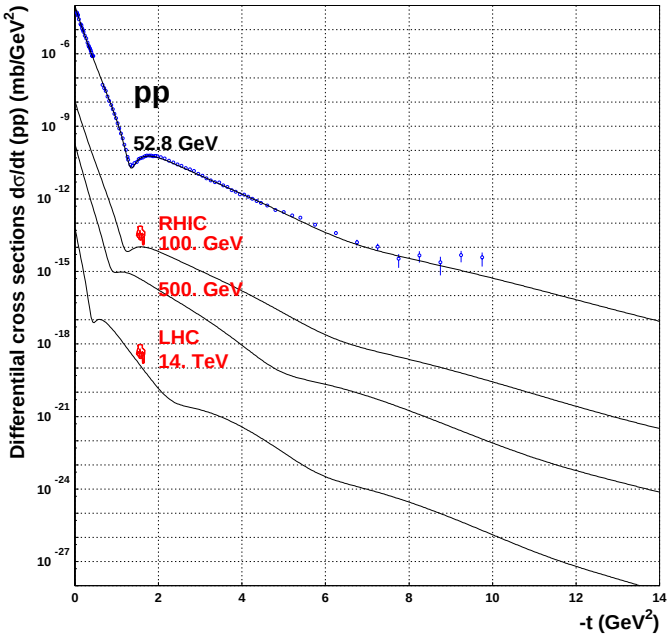

Fig. 13. Predictions of the three pomeron model for the differential cross-section of pp scattering which will be measured at LHC with $s^{1/2} = 14.\,\text{TeV}$ and at RHIC $s^{1/2} = 100.\,\text{GeV}$ and $s^{1/2} = 500.\,\text{GeV}$. The data corresponding to the energy $s^{1/2} = 52.8\,\text{GeV}$ is multiplied by 10^{-6}, RHIC at 500 GeV by 10^{-10}, RHIC at 500 GeV by 10^{-12}, and that of LHC by 10^{-16}

$$\begin{aligned}\sqrt{s} &= 14.\,\text{TeV},\\ \sigma_{\text{tot}}^{pp} &= 106.73\,\text{mb}^{+7.56\,\text{mb}}_{-8.50\,\text{mb}},\\ \sigma_{\text{elastic}}^{pp} &= 29.19\,\text{mb}^{+3.58\,\text{mb}}_{-2.83\,\text{mb}},\\ \rho^{pp} &= 0.1378^{+0.0042}_{-0.0061}.\end{aligned} \tag{17}$$

Predictions for RHIC are

$$\begin{aligned}\sqrt{s} &= 100.\,\text{GeV},\\ \sigma_{\text{tot}}^{pp} &= 45.96\,\text{mb}^{+1.41\,\text{mb}}_{-1.38\,\text{mb}},\\ \sigma_{\text{elastic}}^{pp} &= 8.40\,\text{mb}^{+0.34\,\text{mb}}_{-0.32\,\text{mb}},\\ \rho^{pp} &= 0.0962^{+0.0032}_{-0.0032};\end{aligned} \tag{18}$$

$$\begin{aligned}\sqrt{s} &= 500.\,\text{GeV},\\ \sigma_{\text{tot}}^{pp} &= 59.05\,\text{mb}^{+2.94\,\text{mb}}_{-3.10\,\text{mb}},\\ \sigma_{\text{elastic}}^{pp} &= 12.29\,\text{mb}^{+0.79\,\text{mb}}_{-0.76\,\text{mb}},\\ \rho^{pp} &= 0.1327^{+0.0052}_{-0.0071}.\end{aligned} \tag{19}$$

The parameters of the pomeron trajectories are

$$\begin{aligned}\alpha(0)_{\mathbb{P}_1} &= 1.058, \quad \alpha'(0)_{\mathbb{P}_1} = 0.560\,\text{GeV}^{-2};\\ \alpha(0)_{\mathbb{P}_2} &= 1.167, \quad \alpha'(0)_{\mathbb{P}_2} = 0.273\,\text{GeV}^{-2};\\ \alpha(0)_{\mathbb{P}_3} &= 1.203, \quad \alpha'(0)_{\mathbb{P}_3} = 0.094\,\text{GeV}^{-2}.\end{aligned} \tag{20}$$

Their coupling constants obey the following inequality:

$$c_{\mathbb{P}_1} > c_{\mathbb{P}_2} > c_{\mathbb{P}_3}. \tag{21}$$

The intercepts and slopes obey the following inequalities:

$$\begin{aligned}\Delta_{\mathbb{P}_1} &< \Delta_{\mathbb{P}_2} < \Delta_{\mathbb{P}_3}\\ \alpha'_{\mathbb{P}_1}(0) &> \alpha'_{\mathbb{P}_2}(0) > \alpha'_{\mathbb{P}_3}(0),\end{aligned} \tag{22}$$

i.e. the higher the intercept is, the lower is the slope. In other terms the pomeron with higher intercept is "harder" in the sense that it is associated with shorter distances defined by the slope. We also observe an interesting feature: the product of the intercept and the slope is approximately the same for all the pomerons, $\Delta \cdot \alpha'(0) \simeq 0.040 \pm 0.0009\,\text{GeV}^{-2}$. This is seen in Fig. 14. This constant seems surprisingly universal if compared with the products of other reggeon parameters used in this model (Fig. 15). At present we have no clear understanding of this universality.

We can only remind the reader that the high energy asymptotic behaviors of the total and elastic cross-sections in the Regge-eikonal approach have the following form:

$$\begin{aligned}\sigma_{\text{tot}}(s)|_{s\to\infty} &\to 8\pi\alpha'_{\mathbb{P}}(0)\Delta_{\mathbb{P}}\ln^2(s/s_0),\\ \sigma_{\text{elastic}}(s)|_{s\to\infty} &\to 4\pi\alpha'_{\mathbb{P}}(0)\Delta_{\mathbb{P}}\ln^2(s/s_0),\end{aligned} \tag{23}$$

and the constant $\alpha'_{\mathbb{P}}(0)\Delta_{\mathbb{P}}\,\text{GeV}^{-2}$ ($\mathbb{P}$ stands for the rightmost singularity of the eikonal function in the J-plane) defines a universal (independent on colliding beams) asymptotic behavior.

It is interesting to enlist the following characteristic properties of the pomerons used in this paper.

The first of the pomerons ("pomeron$_1$") possesses the properties that we expect from the string picture [17] of reggeons, i.e. $\alpha'(0)_{\mathbb{P}} = (1/2)\alpha'(0)_f = 0.42\,\text{GeV}^{-2}$ and indeed $\alpha'(0)_{\mathbb{P}_1} = 0.559 \pm 0.078\,\text{GeV}^{-2}$.

The second pomeron ("pomeron$_2$") is close to what is called the "supercritical pomeron" with the slope $\alpha'(0)_{\mathbb{P}_2} = 0.273 \pm 0.005\,\text{GeV}^{-2}$ close to its "world" value $\alpha'(0)_{\mathbb{P}} \simeq 0.25\,\text{GeV}^{-2}$.

The third pomeron ("pomeron$_3$") is reminiscent of what is known as a "hard" (or perturbative QCD) pomeron. Its parameters ($\alpha(0)_{\mathbb{P}_3} = 1.203$, $\alpha'(0)_{\mathbb{P}_3} = 0.094\,\text{GeV}^{-2}$) are close to the calculated parameters of the perturbative pomeron, which arise from the summation of reggeized gluon ladders and BFKL equation [18]: $\alpha(0)_{\mathbb{P}}^{\text{BFKL}} \simeq 1.2$, $\alpha'(0)_{\mathbb{P}}^{\text{BFKL}} \sim 0.\,\text{GeV}^{-2}$. The fact that a "hard" pomeron arises in a presumably "soft" framework may seem quite unexpected. However we are not particularly inclined to identify straightforwardly our "hard pomeron" with that which is the subject of perturbative QCD studies.

The odderon has the following parameters: $\alpha(0)_{\mathbb{O}} = 1.192$, $\alpha'(0)_{\mathbb{O}} = 0.048\,\text{GeV}^{-2}$ in agreement with the unitarity constraints (15). The odderon intercept is positive and close to that of pomeron$_3$. The slope is almost zero. The coupling is so small that only high-t data may be sensible to the odderon contribution.

Assuming that one can neglect the non-linearities of the Regge trajectories and making use of the simple parametrization

$$\alpha(m^2) = \alpha(0) + \alpha'(0)\cdot m^2, \tag{24}$$

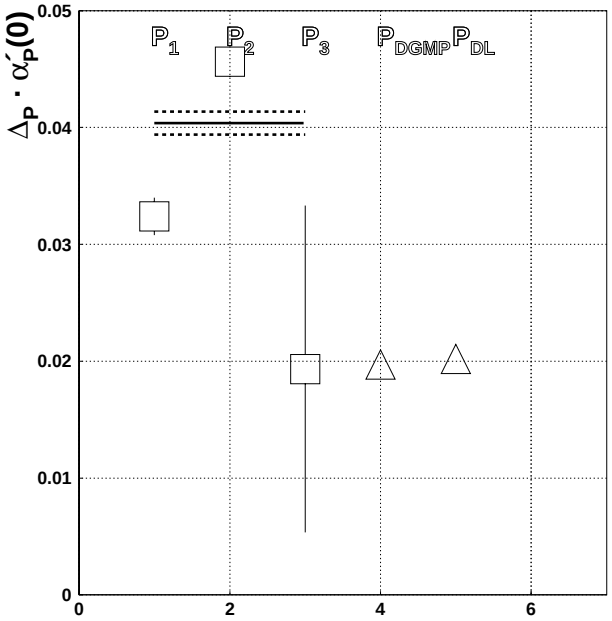

Fig. 14. Products of intercepts to slopes for the pomerons (hollow squares) and the pomeron in a generalized eikonalization model $\mathbb{P}_{\rm DGMP}$ [6], Donnachie and Landshoff supercritical pomeron $\mathbb{P}_{\rm DL}$ [14] (hollow triangles). The solid line corresponds to the mean value of the product (for the three pomerons) and dashed lines correspond to its error corridor

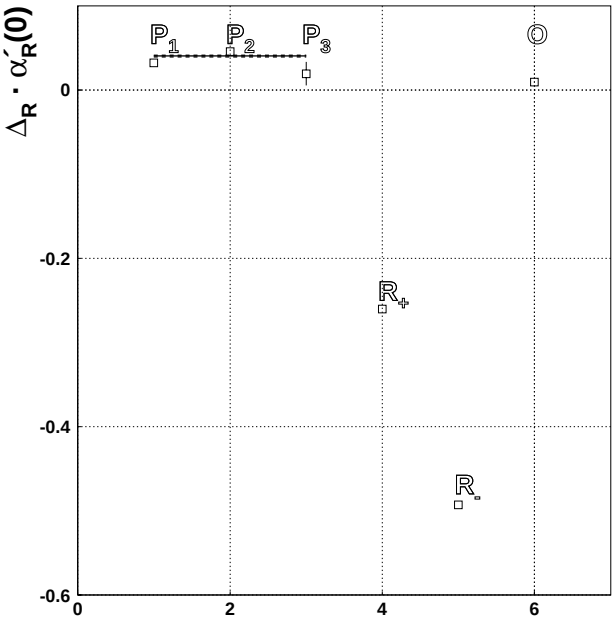

Fig. 15. Products of intercepts to slopes for the pomerons, the odderon, and reggeons used in the present model

we can try to estimate the corresponding spectroscopic content of our model.

Then $\mathrm{Re}\alpha(m^2) = J$, where J is an integer number corresponding to the spin of the particle which we should find lying on the trajectory.

The trajectories are depicted in Fig. 16. The $C+$ reggeon trajectory is in fact a combination of two families of

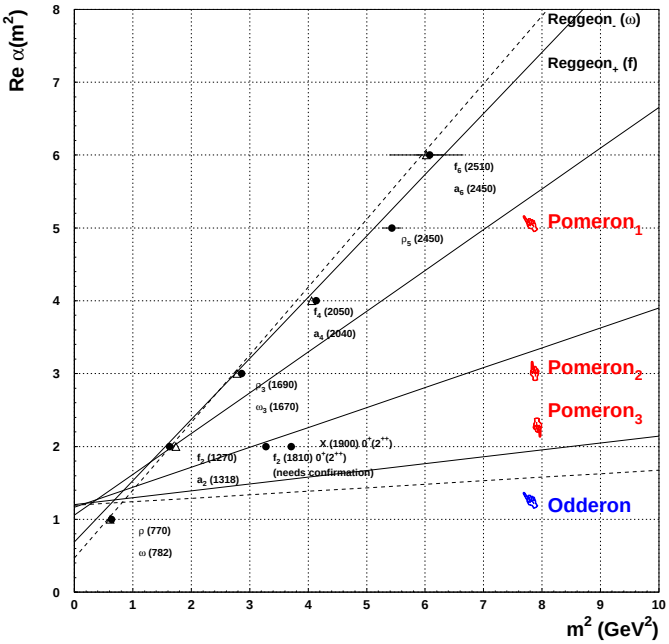

Fig. 16. Regge trajectories of secondary reggeons, three pomerons and the odderon

mesons f and a_2. The $C-$ reggeon trajectory is a combination of two families of mesons ω and ρ. As is seen, the secondary reggeon trajectories fairly well describe the spectrum of mesons.

Among the mesons with appropriate quantum numbers there exist two that fit the pomeron trajectory (0^+ J^{++}): $f_2(1810)$ 0^+2^{++} with mass $m = 1815 \pm 12$ MeV and $X(1900)$ 0^+2^{++} with mass $m = 1926 \pm 12$ MeV. One of them is supposed to be on the pomeron$_2$ trajectory.

Returning to our "polypomeron" hypothesis it is fairly natural to ask: what happens if one admits a fourth etc. pomeron? Is there some optimum in the number of "relevant" pomerons above which the quality of description is not improved much? And, finally, what is the underlying physics of such a construction? We hope very much to be able to answer at least some of these questions in the nearest future.

Acknowledgements. We would like to thank Maurice Giffon for comments, Enrico Predazzi for useful discussions and for critical reading of the manuscript and Munir Islam for fruitful discussions and suggestions improving the presentation.

References

1. V.A. Petrov, A.V. Prokudin, S.M. Troshin, N.E. Tyurin, hep-ph/0103257; submitted to J. Phys. G
2. A. Faus-Golfe, J. Velasco, M. Haguenauer, hep-ex/0102011
3. Pierre Gauron, Basarab Nicolescu, Phys. Lett. B **486**, 71 (2000), hep-ph/0004066
4. K. Kontros, A. Lengyel, Z. Tarics, hep-ph/0011398
5. A. Donnachie, P.V. Landshoff, Phys. Lett. B **437**, 408 (1998)

6. P. Desgrolard, M. Giffon, E. Martynov, E. Predazzi Eur. Phys. J. C **16**, 499 (2000)
7. M.M. Block, E.M. Gregores, F. Halzen, G. Pancheri Phys. Rev. Lett. D **60**, 054024 (1999)
8. A.K. Likhoded, O.P. Yushchenko, Int. J. Mod. Phys. A **6**, 913 (1991)
9. L.N. Lipatov, Yad. Fiz. **23**, 642 (1976); Sov. J. Nucl. Phys. **23**, 338 (1976)
10. V.A. Petrov, A.V. Prokudin, in Proceedings of the International Conference on Elastic and Diffractive Scattering (VIIIth Blois Workshop) June 28–July 2, 1999 Protvino, Russia (World Scientific Publishing, Singapore 2000), p. 95; hep-ph/9912245
11. R.J.M. Covolan, P. Desgrolard, M. Giffon, L.L. Jenkovszky, E. Predazzi, Z. Phys. C **58**, 109 (1993)
12. M. Froissart, Phys. Rev. D **123**, 1053 (1961); A. Martin, Phys. Rev. D **129**, 993 (1963)
13. M. Giffon, E. Martynov, E. Predazzi, Z. Phys. C **76**, 155 (1997); J. Finkelstein, H.M. Fried, K. Kang, C.-I. Tan, Nucl. Phys. B **232**, 257 (1989); E. Martynov, Phys. Lett. B **267**, 257 (1989); H.M. Fried, in Functional Methods and Eikonal Models (Editions Frontières, 1990) p. 214
14. A. Donnachie, P.V. Landshoff, Phys. Lett. B **296**, 227 (1992)
15. C. Bourelly, J. Soffer, T.T. Wu, Phys. Rev. D **19**, 3249 (1979); C. Bourelly, J. Soffer, T.T. Wu, Phys. Rev. Lett. **54**, 757 (1985)
16. M.M. Islam, I. Innocente, T. Fearnley, G. Sanguinetti, Europhys. Lett. **4**, 189 (1987)
17. L.D. Soloviev, hep-ph/0006010; Theor. Math. Fiz. **126**, 247 (2001); ibid. **126**, 203 (2001)
18. V.S. Fadin, L.N. Lipatov, Phys. Lett. B **429**, 127 (1998); Marcello Ciafaloni, Gianni Camici, Phys. Lett. B **430**, 349 (1998); D.A. Ross, Phys. Lett. B **431**, 161 (1998)